Effect of Urea Links in the Backbone of Polyimide Aerogels

Baochau N. Nguyen[*†], Daniel A. Scheiman*[*†], Mary Ann B. Meador [‡], Jiao Guo[φ], Bart Hamilton[φ] and Linda S. McCorkle[†]*

University Space Research Association, 7178 Columbia Gateway Drive, Columbia, MD 21048;

NASA Glenn Research Center, 21000 Brookpark Road, Cleveland OH 44135

University of Akron, 250 South Forge Street, Akron OH 44325

TITLE RUNNING HEAD: aerogels, polyimide and poly(imide-urea), flexible, high-temperature.

ABSTRACT. Flexible, conformal polyimide aerogels with low density, good mechanical properties and high surface areas have attracted much attention for many potential applications such as lightweight antenna substrates, insulating materials for launch vehicles, inflatable structures, aircraft or space suits. Development and improvements to fabrication of polyimide aerogel thin films have been reported over the last decade to meet the

[*] To whom correspondence should be addressed: baochau.n.nguyen@nasa.gov; daniel.a.scheiman@nasa.gov

[†] University Space Research Association,

[‡] NASA Glenn Research Center

[φ] University of Akron.

needs of many of these applications. However, most starting materials are expensive. In this research, we utilized commercially available, low cost monomers including 4,4'-bis(4-aminophenoxy)propane (BAPP) and 3,3',4,4'-benzophenone tetracarboxylic dianhydride (BTDA), and 4,4-methylene diphenyl di-isocyanate (MDI) in fabricating polyimide (PI) and polyimide-urea (PIU), which were then cross-linked with 1,3,5-tris(4-aminophenoxy)benzene (TAB). It was found that the addition of MDI into the PI chains not only maintained the flexibility of the aerogel films, but also enhanced the film casting, allowing the production on pilot scale. With the capability in producing robust films at affordable cost, application of the PIU aerogel films can be expanded to terrestrial goods such as winter clothing, or pipe wrapping, etc. In addition, the presence of only a small addition of the urea links in the polyimide chains in PIU aerogels led to lower shrinkage when compared to the corresponding PI aerogels, leading to lower density.

Key words: aerogels; polyimides, polyimide-urea, di-isocyanate; hybrid materials; flexible films; thermal stability.

Introduction

Aerogels are highly porous materials filled with up to 99.8 % air.[1,2] They possess many unique features such as high surface area, small pore size,[3,4] low dielectric constant[5,6] and low thermal conductivity.[7,8] These features lead to many potential uses of aerogels, including as insulation for space suits and habitats and inflatable decelerators for entry descent and landing,[9] as well as lightweight substrates for high performance antennas.[10] Many different types of aerogels have been developed, including silica,[11] boron nitride,[12] alumina,[13] hybrid inorganic-organic,[14,15,16] carbon,[17,18,19] graphene,[20,21] cellulose based,[22,23] different organic polymers[24,25] and polymer composites,[26,27] to name a few.

Over the last decade, aromatic polyimide aerogels have been of great interest due to their excellent thermal stability, high use temperature and superior mechanical properties.[28, 29, 30] The properties of these PI aerogels can be tailored for specific applications by selective use of the dianhydrides, diamines, and cross-linkers. For example, changing the diamine from p-phenylene diamine (PPDA) or 4,4'-oxydianiline (ODA) to 2,2'-dimethylbenzidine

(DMBZ), or a combinations of each can be used to modify the rigidity or flexibility.[31] Introducing a spacer with aliphatic linkages up to 12 methyl units,[32, 33] or linkages like the neopentyl group in 1,3-bis(4-aminophenoxy)-2,2-dimethylpropane (BAPN)[34] will alter hydrophobicity and mechanical properties. Another attractive feature of polyimide aerogels is the low dielectric constant. It has been shown that lower dielectric constant is obtained as the density of aerogel decreases, regardless of monomers.[35] Thus, aerogel films with thicknesses from 0.5 mm[36] to 2 mm using the aliphatic linkages have been demonstrated with potential application for inflatable decelerators and extra-vehicular activity (EVA) space suits,[37] etc. and as substrates for lightweight, high performance conformal antennas,[32-34] respectively. The optical transparency of PI aerogels can be modified using pyromellitic dianhydride (PMDA) and 4,4'-hexafluoroisopropylidene di(phthalic anhydride) (6FDA) in combination with DMBZ and might be useful as light filter in addition to thermal insulation in window panes.[29]

Multifunctional amines, anhydrides and isocyanates have all been utilized to create three-dimensional (3-D) or cross-linked aerogel networks. Examples of cross-linkers include octa-aminophenylsilsesquioxane (OAPS),[31] 1,3,5-triaminophenoxybenzene (TAB),[31-33] 1,3,5-tris(aminophenyl) benzene (TAPB),[38] 2,4,6-tris(4-aminophenyl)pyridine (TAPP),[39] 1,3,5-benzenetricarbonyl trichloride (BTC),[40,29]poly(maleic anhydride)s (PMAs)[41] and Desmodur N3300A (a hexamethylene diisocyanate base (HDI) trimer).[28] Properties of cross-linked polyimide aerogels with backbones based on the diamines ODA, DMBZ, PPDA and dianhydrides BPDA, 6FDA and PMDA [31, 42, 43] have been extensively investigated. While the dianhydride 3,3',4,4'-benzophenone tetracarboxylic dianhydride (BTDA) or the diamine 2,2-bis(4-[4-aminophenoxy]phenyl)propane (BAPP) have high solubility in the commonly used solvent NMP and are commercially available at a relatively low cost, few researchers have studied alternative PI aerogels using BTDA and BAPP. An early study found using polyimide made from BTDA and BAPP as a cross-linker for silica aerogels helped to improved mechanical properties.[16] A later study by Meador *et.al.*, showed that TAB-cross-linked polyimide aerogels made with BTDA were similar in mechanical properties to those made using BPDA, while surface areas tended to be higher with BTDA.[44]

The hydrophobicity of BPDA-ODA based aerogels were greatly improved by using at least 50 % DMBZ in place of ODA, as previously reported by Guo *et.al.*[31] A similar effect was observed when replacing ODA with BAPP. [45] It has been shown that BAPP, with ether linkages between the phenyl rings and the central isopropyl unit, tends to improve flexibility and enhance hydrophobicity PI aerogels than ODA[42]

It has been demonstrated that polyimide-polyurea (PI-PU) copolymers consisting of PMDA, ODA and 4,4'-methylene bis(phenyl isocyanate) (MDI) lowered the dielectric constant as the mole ratio of polyurea in the co-polymers was increased.[46] Hydrogen bonding from urea groups was also believed to cause chain alignment which increased modulus. In a study conducted by Shinko et. al.,[47] the extent of hydrogen bonds in the cross-linked polyurea aerogels consisted of MDI and a more flexible diamine ODA was found to reduce shrinkage when compared to a more rigid diamine DMBZ.

In this paper, we report the development of PI aerogels prepared from BTDA, BAPP, and cross-linked with TAB. Because BAPP has two ether links and an isopropyl link, it is expected to provide flexibility in the polyimide backbone. In addition, since including polyurea in polyimide chains enhances mechanical properties as mentioned above,[44] it is of interest to study the effect of the urea link in the PI aerogels using MDI as the di-isocyanate. An advantage of the selected monomers utilized in this study, BTDA, BAPP and MDI, is that they are commercially available at low cost. Morphology, surface area, physical and mechanical properties, as well as thermal oxidative stability at 150 °C and 200 °C up to 500 hours of these PI aerogels and their PIU aerogel analogs were evaluated, characterized and compared.

Experimental procedures

Materials. Precursors 3,3',4,4'-Benzophenone tetracarboxylic dianhydride (BTDA) and 2,2-bis(4-[4-aminophenoxy]phenyl)propane (BAPP) were purchased from Chriskev Company, Inc. and Wakayama Seika Kogya Com., Lmt., respectively; 1,3,5-tris(4-aminophenoxy) benzene (TAB) was custom synthesized by Oakwood Chemical; and 4,4'-methylene-bis-diphenyldiisocyanate (MDI) was provided by Bayer. N-

methylpyrrolidinone (NMP, HPLC grade) was obtained from Tedia; acetone (HPLC grade) was from Pharmco Aaper; and liquid carbon dioxide was from Air Gas, acetic anhydride (AA) and pyridine (Py) were purchased from Aldrich. BTDA was vacuum dried overnight at 140°C before use.

All the cross-linked polyimide (PI) (Scheme 1) and poly(imide-urea) (PIU) aerogels (Scheme 2) were prepared at 10 w/w% total solution, including NMP, acetic anhydride and pyridine The lengths of the oligomer segments were formulated with imide repeating unit, n, of 6, 12, 18, 24 and 30. The reactions were completed at room temperature using a chemical imidization process.

Synthesis of cross-linked polyimide aerogels. The polyimide (PI) aerogels (Scheme 1) were made by reacting BAPP and BTDA with a mole ratio of n:(n + 1), respectively, forming an anhydride end capped oligomer poly(amic acid) [**I**]. The triamine TAB was then added, followed by the addition of acetic anhydride and pyridine to form a three-dimensional polyimide network [**II**]. An example for the preparation of the cross-linked polyimide gels made with an n value of 12 is as follows: BTDA (2.35 g, 7.29 mmol) was added to 26.75 ml of NMP at room temperature and stirred until it dissolved. BAPP (2.76 g, 6.73 mmol) was then added and stirred until dissolved. TAB (0.15 g, 0.374 mmol), was first dissolved in 5 ml of NMP and then added to the BAPP-BTDA oligomer solution. This solution was stirred until homogenous, acetic anhydride (AA) (5.10 ml) and pyridine (4.35 ml) were added in sequence while continuing to stir. The resulting cross-linked polyimide solution was poured into cylindrical molds and allowed to gel or cast into thin films after 45-48 minutes and then allowed to finish gelation. Gelation finished within 50 min.

Synthesis of poly(imide-urea) aerogels. The poly(imide-urea) aerogels were formulated according to Scheme 2. Theoretically, one equivalent mole of BTDA was replaced with one equivalent mole of MDI per n-formulated polymer chain. The urea precursor then reacts with two BAPP amines and is incorporated into the oligomer before being cross-linked with TAB, analogous to the n-formulated PI aerogels undergoes. Thus, one equivalent mole of MDI was first reacted with n equivalent moles of BAPP to form an amine capped MDI [**III**] in an excess of BAPP. The mixture was then reacted with n equivalent moles of BTDA, forming a dianhydride capped (amic

acid-urea) oligomer with MDI in the polymer backbone [**IV**]. The oligomers were cross-linked with TAB at a mole ratio of 3:2, respectively, and were chemically imidized, creating a three-dimensional poly(imide-urea) [**V**]. A typical reaction with 12 repeating imide units was carried out as follows: MDI (0.14 g, 0.563 mmol) was dissolved in 26.70 mls of NMP. BAPP (2.78 g, 6.76 mmol) was then added to the solution and stirred until dissolved, followed by the addition of BTDA (2.18 g, 6.76 mmol) forming the (amic acid-urea) oligomer in solution. TAB (0.15 g, 0.38 mmol) was dissolved separately in 5.00 mls of NMP and then poured into the amic acid-urea mixture. Acetic anhydride (5.10 ml) and pyridine (4.40 ml) were then dispensed consecutively and stirred until the solution was homogenous. The resulting solution was poured into cylindrical molds and allowed to gel and/or cast into a thin film approximately 15 minutes after the addition of pyridine. Gelation finished at 25 minutes.

The molds were prepared from 20-ml, 2 cm diameter plastic syringes having the needle ends cut off with the plunger extended down. The PI aerogel films were cast using an EC-100 EZ coater at a fixed speed of 119 cm/min with the doctor blade gauge set at 0.991 mm. It was noticed that the BTDA-BAPP amic acid was quite viscous while stirring but reduced substantially after the addition of acetic anhydride (AA) pyridine. The viscosity of the PI solutions remained relatively low near the gelation point, then increased rapidly, resulting in a shorter time for the casting of films, consequently limiting the PI aerogel films size to about 3" x 6" films. This observation of the change in viscosity is in agreement with a study investigated by Chuang et.al.[48] In contrast, the viscosity of the BTDA-BAPP amic acid having MDI in the backbone was less viscous than that of the PI solution before being converted to PIU. After the addition of AA and pyridine, the viscosity of the PIU solution continuously increased. Therefore, larger thin films with size of 12-inch wide and up to 5-feet long were able to be cast using a roll-to-roll HED International Pro-Cast model number TCM-252SM at a speed of 80 cm/min with the doctor blade set at 0.889 mm. Both the PI and the PIU solutions were cast on to a PET film as a carrier and then covered with PE film to prevent evaporation of solvents. The gels were either demolded or peeled off the film carrier after being allowed to age overnight at room temperature before starting the solvent exchange process.

NMP, acetic anhydride and pyridine were washed out gradually with full volume solvent exchanges twice daily in 6 – 18-hour intervals in between washes with acetone/NMP solutions initially at 25/75 vol/vol ratios, followed by 75/25 vol/vol ratios, and then four more washes with neat acetone. The cross-linked polyimide aerogels were then supercritically dried using CO_2 extraction of the gels with an Accudyne multi-vessel automated system. The aerogels were then outgassed and post cured under full vacuum at 80 °C for 12 hours before analyses and mechanical testing.

Scheme 1. Proposed synthetic route of cross-linked polyimide aerogel with n = 12.

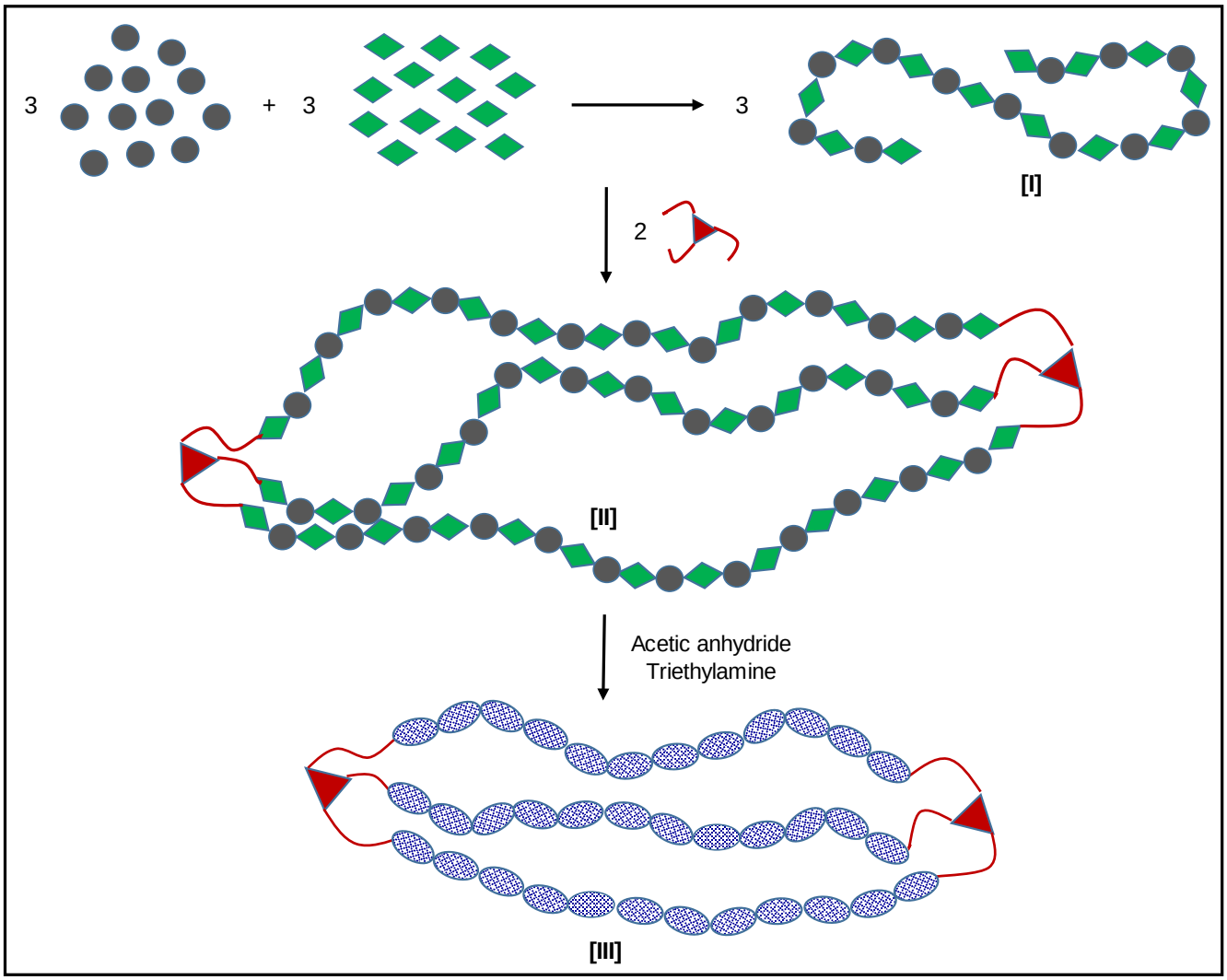

Scheme 2. Proposed synthetic path of cross-linked polyimide-urea aerogel with n = 12.

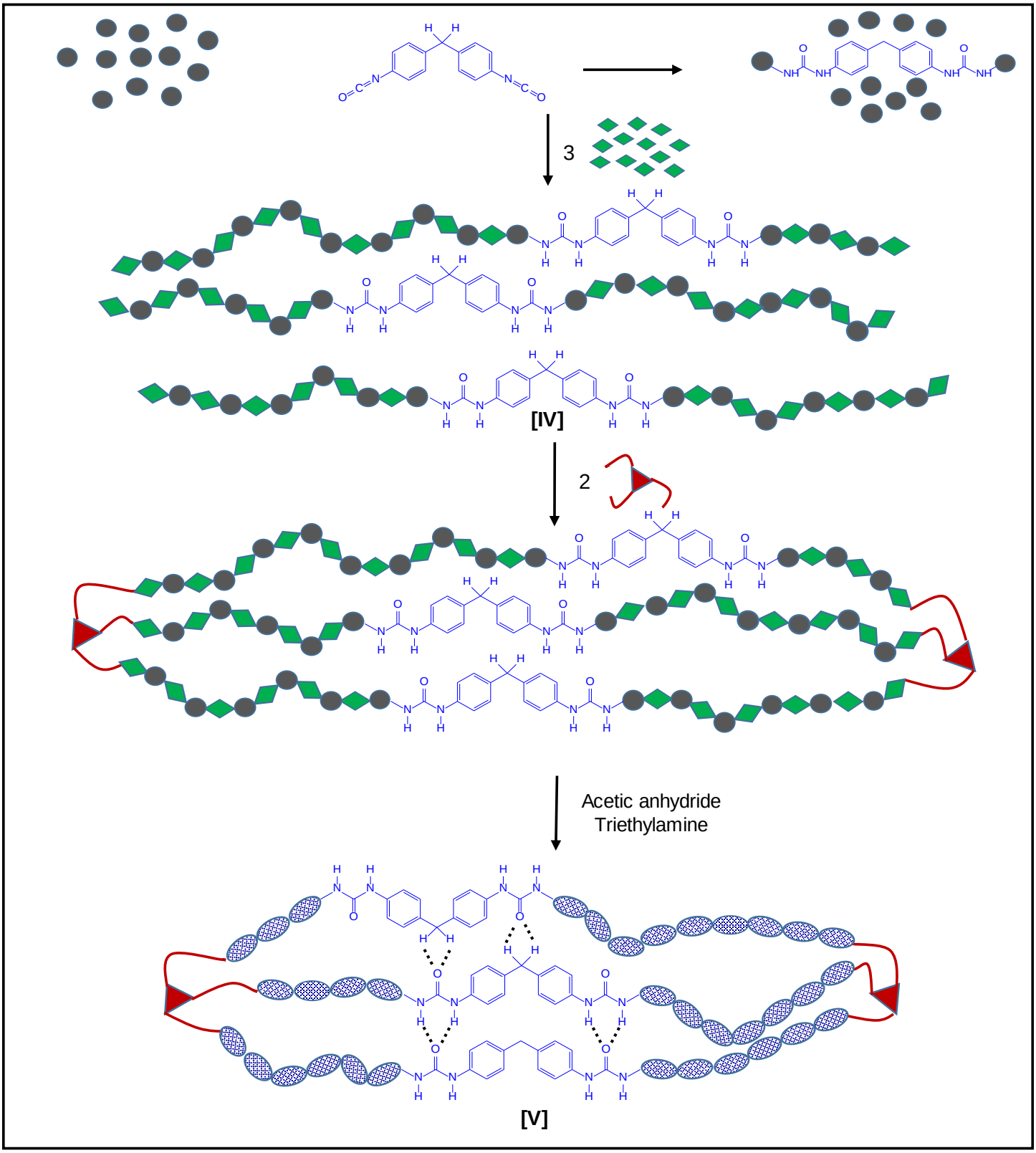

Physical measurements. Brunauer-Emmett-Teller (BET) surface area and Barrett-Joyner-Halenda (BJH) pore size distribution of the dried aerogels were measured for 0.01 to 0.02 g samples using a Micromeritics

ASAP 2020 chemisorption apparatus. Samples for microscopy were sputter coated with gold/palladium and viewed using a Hitachi S-4700-11 field emission scanning electron microscope. Thermal gravimetric analysis (TGA) was performed using a TA Instruments TGA2950. The samples were heated from room temperature to 750 °C at a ramp rate of 10 °C/min under nitrogen with sample sizes ranging from 2 – 8 mg. The bulk density (ρ_b) was determined by measuring the weight and volume of the sample. Dimensional change, or areal shrinkage (%), of monoliths was taken as the difference in diameters between the mold (nominal 20 mm) and the aerogel after being dried under vacuum. Skeletal density was measured using a Micromeritics AccuPyc 1340 helium pycnometer. The porosity (%) of the cross-linked aerogels was calculated using Eq. 1

$$\text{Porosity } (\%) = (1-\rho_b/\rho_s) \times 100\ \% \qquad \text{(Eq. 1)}$$

where ρ_b is bulk density and ρ_s is skeletal density

Solid ^{13}C NMR and Fourier-transform infrared spectroscopy (FTIR) were performed on a Bruker Avance-300 spectrometer and a Thermo Scientific Nicolet 380 FT-IR, respectively.

Mechanical testing. The compression modulus of the aerogels was tested on a monolith cylinder with a length to diameter ratio of 1.25-1.50 to 1, using an Instron model 4505. The samples were compressed dimensionally with a 2.25 kN load cell at 0.05 in/min, as per ASTM D695-10 standard. Tensile properties of the aerogel films and their flexibility were analyzed from data collected using a TA instruments DMA Q800.

Isothermal study. Cross-linked PI and cross-linked PIU specimens with thickness of 0.5 – 1.0 mm were placed in an oven and isothermally aged at 150 °C and 200 °C for up to 500 hours in air. Shrinkage measurements based on dimensional changes were taken at timed intervals of 1, 3, 6, 9, 12, 18, 24, 48, 72, 100, 200, 300, 400 and 500 hours.

Statistical Analysis. In the experimental study, all physical and mechanical properties were modeled and analyzed using Stat-Ease software Design-Expert 12. A quadratic design was used with 18 different experimental runs for cylindrical samples (Table 1) and 16 for films (Table 2), including 1-3 repeats for the PIU

formulations to analyze model reliability and accuracy. Statistical analysis was conducted using backward stepwise regression removing insignificant terms ($p < 0.1$) from the model one at a time. Standard deviations reported are errors obtained from this multiple linear analysis of the pooled data. Graphs derived from this model are shown in Figures 3, 4, 6, 8, S1 and S2. The lines and error bars on the plots are derived from multiple linear regression analysis of the entire dataset.

Results and Discussion

Two sets of cross-linked polyimide (PI) and poly(imide-urea) (PIU) aerogels were synthesized using acetic anhydride and pyridine to catalyze chemical imidization at room temperature. All the aerogels were prepared in 10 wt% solutions in NMP according to Scheme 1 for PI aerogels and Scheme 2 for PIU aerogels. Only one equivalent of MDI was used in place of one equivalent of BTDA in the PIU formulations. Thus, changes reported herein are by including only a small amount of urea in the PI backbone.

Table 1. Physical and mechanical properties of polyimide and poly(imide-urea) aerogels in cylindrical form.

Chain length n	MDI	Shrinkage %	Porosity %	Density g/cm^3	BET m^2/g	Compression modulus, MPa	Specific modulus, $MPa/(kg/m^3)$
6	no	26.0	82	0.26	465	62.0	238.5
12	no	25.4	82	0.25	462	69.7	278.8
18	no	29.4	79	0.30	373	92.6	308.7
24	no	31.0	77	0.31	356	67.2	216.8
30	no	31.5	77	0.32	389	106.7	333.4
6	yes	23.0	85	0.20	484	22.4	112.0
6	yes	21.2	85	0.20		24.6	123.0
12	yes	24.0	83	0.23	409	30.6	133.0
12	yes	21.5	85	0.20	473	22.6	133.0
12	yes	23.5	84	0.22	475		
18	yes	19.4	83	0.24	425	38.2	159.2
18	yes	25.9	82	0.22	462	39.2	178.2
18	yes	24.2	83	0.23	462	35.5	154.3
24	yes	21.8	85	0.21	463	33.7	160.5
24	yes	26.3	82	0.24	528	42.8	178.3
30	yes	24.1	83	0.23	458	37.8	164.3
30	yes	22.6	84	0.21	468		
30	yes	22.2	85	0.21	513		

Table 2. Physical and mechanical properties of polyimide and poly(imide-urea) aerogels in film form.

Chain length n	MDI No/yes	Film density g/cm^3	Film tensile modulus, MPa	Specific modulus, MPa/(kg/m^3)
6	no	0.31	118.1	381.0
12	no	0.29	92.7	319.7
18	no	0.34	133.1	391.5
24	no	0.39	157.8	404.6
30	no	0.38	174.4	458.9
6	yes	0.27	65.0	240.7
6	yes	0.29	71.2	245.5
12	yes	0.28	61.0	217.9
12	yes	0.26	62.6	240.8
18	yes	~~0.29~~	82.1	283.1
18	yes	~~0.29~~	79.4	273.8
18	yes	0.32	75.9	237.2
24	yes	0.32	93.5	292.2
24	yes	~~0.34~~	93.0	273.5
30	yes	0.31	76.3	246.1
30	yes	0.33	73.9	223.9

Shown in Figures 1 (a-b) are the ^{13}C NMR spectra of polyimide and poly(imide-urea) aerogels with an n value of 6 (Fig. 1 a-b). For comparison, the height of the peak at 194 ppm (1) was used to normalize the spectra. The peak at 194 ppm corresponds to the carbonyl (-C=O)- in BTDA.[49] The peak at 164 ppm (2) is the imide carbonyls. The peak centered at 157 ppm (3) is assigned to the urea carbonyl [50,51] and the carbon next to the aromatic ether from BAPP. [52,53,] The peak at 148 ppm (4) corresponds to the aromatic carbon connecting to the isopropyl group. Peaks shown at 42 ppm (5) and 28 ppm (6) are assigned to the isopropyl group from the BAPP, which are in

agreement with the findings in the literature.[53,51] A small increase in intensity is observed at 42 ppm for PIU aerogels due to the methyl group (5) from the MDI.[54,55,56] The peaks ranging from 115 ppm to 140 ppm resonant from the other aromatic carbons found in the backbone. In particular, peaks at 120 ppm (11), 128 ppm (9), and 138 ppm (7) appear to be more defined in the PIU spectra with higher intensity, perhaps due to the attribution of the aromatic rings from MDI. Similarly, the peak centered at 157 ppm (3) seem to be larger, an indication that the urea carbobyl peaks are overlapping with the carbon next to the ether linkage in BAPP.

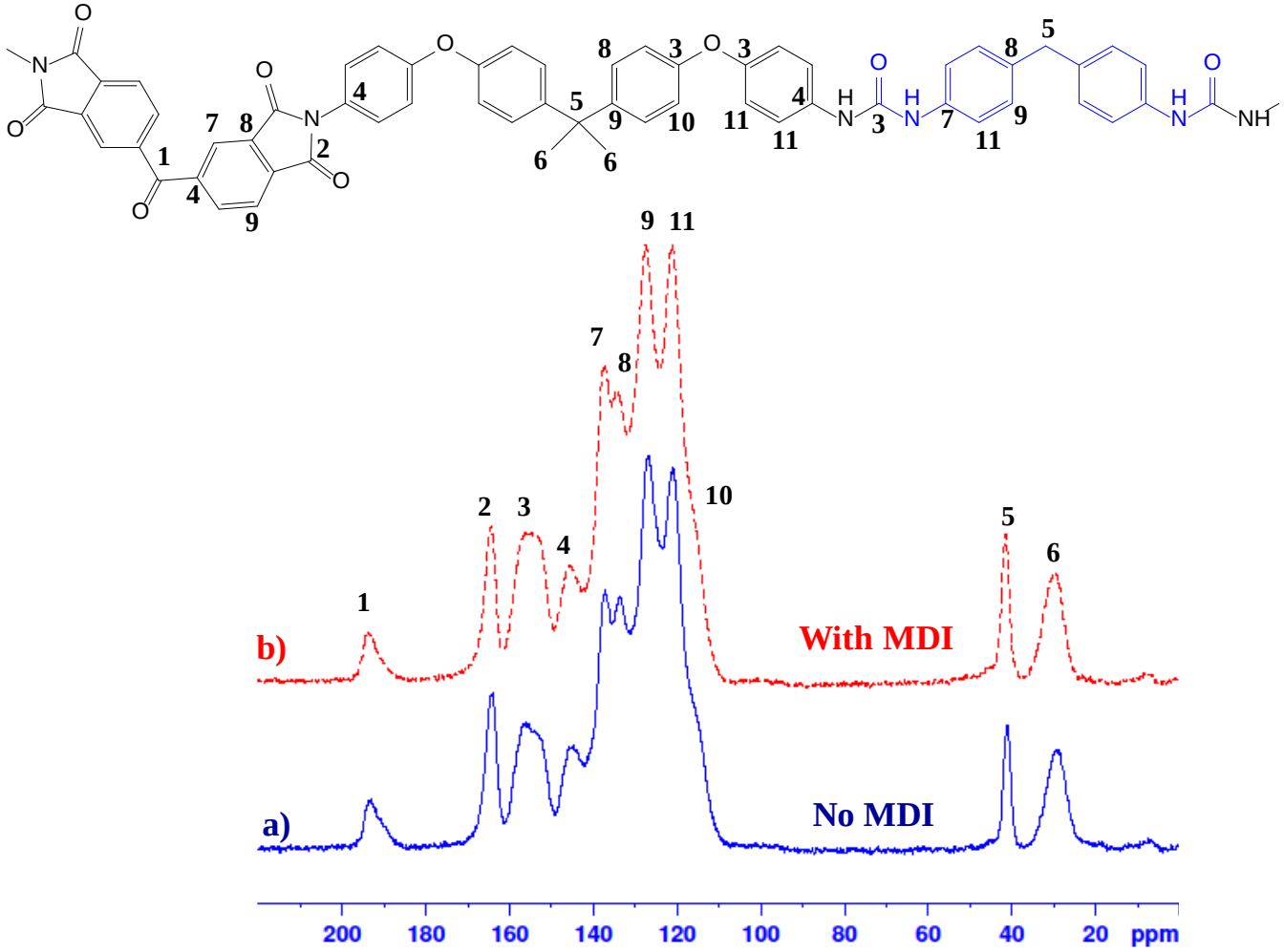

Figure 1. NMR spectra of (a) polyimide aerogel and b) poly(imide-urea) aerogels with an n value of 6.

The chemical bonds of the polyimide and polyimide-urea, with n of 6 (Fig. 2a), were identified using FTIR spectroscopy. The absorbance peaks (cm^{-1}) identified are as listed: the aliphatic moieties,-CH_2, (MDI) and -CH_3

(BAPP), at 2850 to 3150 (w); the imide carbonyls (C=O) at 1780 (w), 1718 (s) and 1380 (m);[45,48] the ether para-substituted phenyl ring from BAPP at 1654 (s), 1600 (w), and 1502 (s), isopropyl para-substituted BAPP at 1240 (s);[52] benzene substitutes from both BAPP, BTDA, and MDI at 1174 (m), 1120 (m), 1090 (m), 1015 (w), 925 (w), 876 (m), 830 (s), 761 (m), 741 (w), 718 (m). The characteristic of urea absorbance is observed at 3200 cm^{-1} - 3450 cm^{-1} for N-H stretching vibration.[57] It also has been reported to be at 1670 cm^{-1} and 1650 cm^{-1} for C=O stretching and 1640 cm^{-1} and 1545 cm^{-1} for bending secondary amine.[46,47,58] Presented in Figure 2b are the FTIR spectrum of n of 6, 18 and 30 on an enlarged scale from 1900 cm^{-1} – 1000 cm^{-1}. As shown, only peak at 1540 cm^{-1} is observed for PIU and its intensity decreases as n increases. Other peaks including peak at 1650 cm^{-1} are associated with BAPP and other moieties, due to many overlapping peaks.

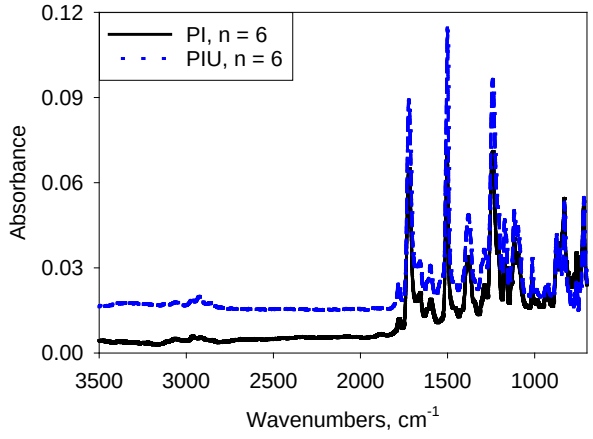

a)

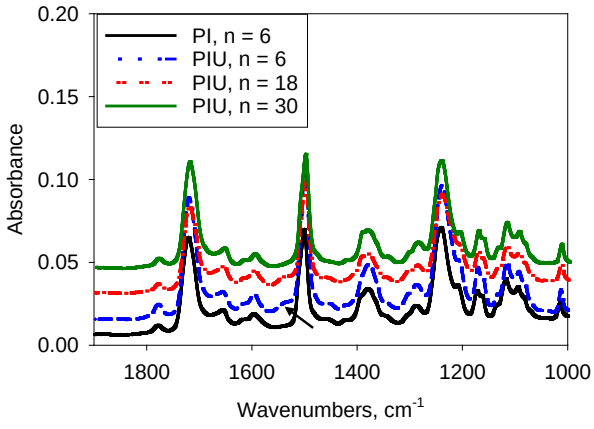

b)

Figure 2. FTIR spectra of polyimide and polyimide-urea aerogel with a) n of 6 on full scale and b) n of 6, 18, and 30 on enlarged scale from 1900 cm^{-1} – 1000 cm^{-1}.

Table 1 contains the data of physical and mechanical properties and characteristics of the PI and PIU aerogels including the areal shrinkage (%), density measurements, porosity, surface area and compressive modulus from the molded aerogels (cylinders), and Table 2 shows the film densities and tensile modulus. Figures 3 (a-b) show graphs of the empirical models for the shrinkage and density of PI and PIU aerogel as a function of the number of repeat units, n. In general, higher shrinkage leads to a higher density, resulting in lower porosity. For the PI aerogels in this study, the shrinkage increases with increasing n value (decreased cross-linking), suggesting the

collapse of pores with longer polymer chains. As the results, the PI aerogels exhibit lower porosity at higher density (Fig. S1). For PIU aerogels, as the n increases, the amount of MDI in the polymer chain decreases. Therefore, it is assumed that the physical properties of PIU aerogels would have similar properties as PI aerogels as n approaches 30. Interestingly, PIU aerogels exhibit lower shrinkage than their PI analogs, and their shrinkages remain relatively constant over the range of n values, leading to lower densities and higher porosities than those of the corresponding PI aerogels (Fig. S1). This may be due to intermolecular hydrogen-bonds from the urea linkages between polymer chains which perform as the secondary cross-linker, as illustrated in Scheme 2. The present of urea linkage in the polymer chains seems to strengthen the nanostructure (make it more resistant to shrinkage) perhaps by acting as secondary crosslinks in the PIU aerogels, even at low concentration.

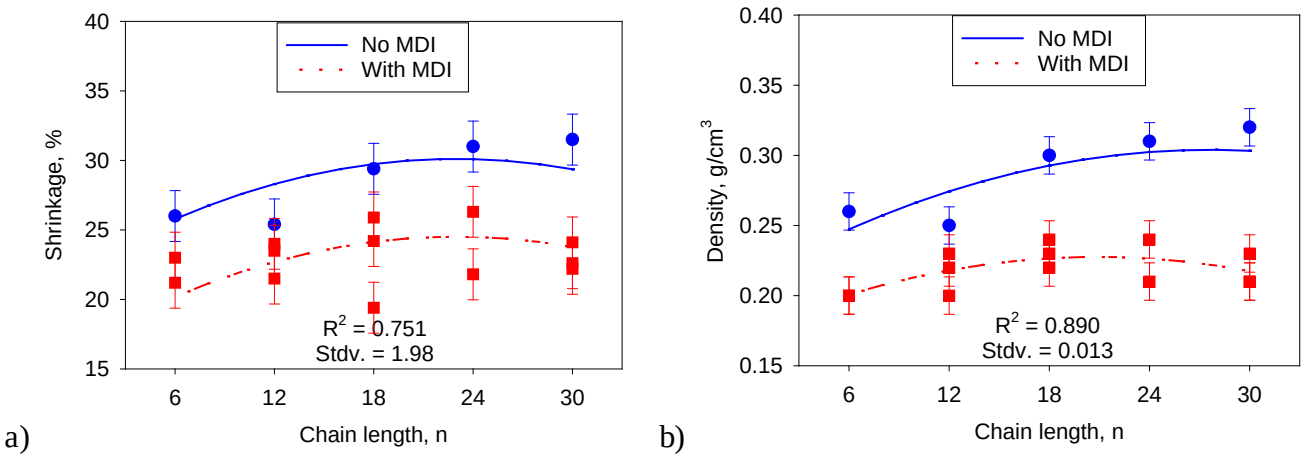

Figure 3. Physical properties of polyimide and poly(imide-urea) aerogels: a) % areal shrinkage and b) density. The lines and error bars on the plots are derived from multiple linear regression analysis of the entire dataset.

Figure 4 shows the BET surface areas for PI and PIU aerogels as a function of n value. The BET surface area follows the same trend as the shrinkage. The surface area of the PI aerogels decreases significantly with increasing n, dropping by about 100 m^2/g over the entire range. In contrast, the surface area for the PIU aerogels are higher than the PI aerogels and nearly unchanged over the range of n. Again, this may be due to the hydrogen bonding between urea groups making the aerogel skeleton more rigid and more resistant to shrinkage and collapsing during processing.

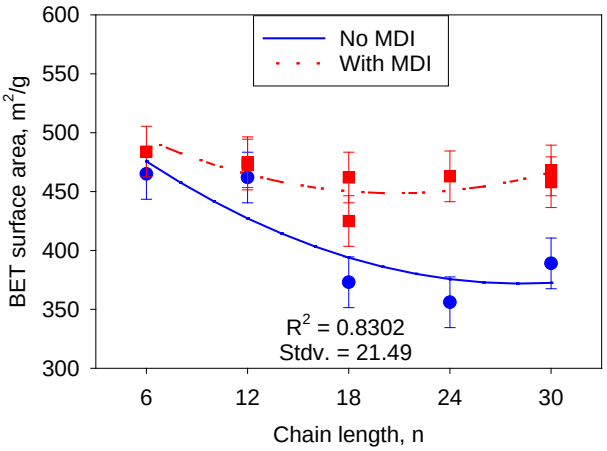

Figure 4. BET surface areas the polyimide and the poly(imide-urea) aerogels. The lines and error bars on the plots are derived from multiple linear regression analysis of the entire dataset.

Scanning electron micrographs (SEM) of the PI (no MDI) and PIU (with MDI) aerogels with n values of 6, and 30 are pictured in Figures 5 (a, c) and Figures 5 (b, d), respectively. The structure of the PI aerogels appears less porous when made using n = 30, compared to those made using n = 6, in keeping with the measured values. In contrast, the PIU aerogels appear more similar at different n, in agreement with the findings for the shrinkage, porosity and BET surface area data. Polymer strands from the PI aerogels appear finer compared to the PIU aerogels which are thicker especially when n = 30. This difference in appearance between PI and PIU aerogels again suggests that the urea linkages derived from MDI act as secondary cross-links through hydrogen-bonds, preventing the structure from collapsing.

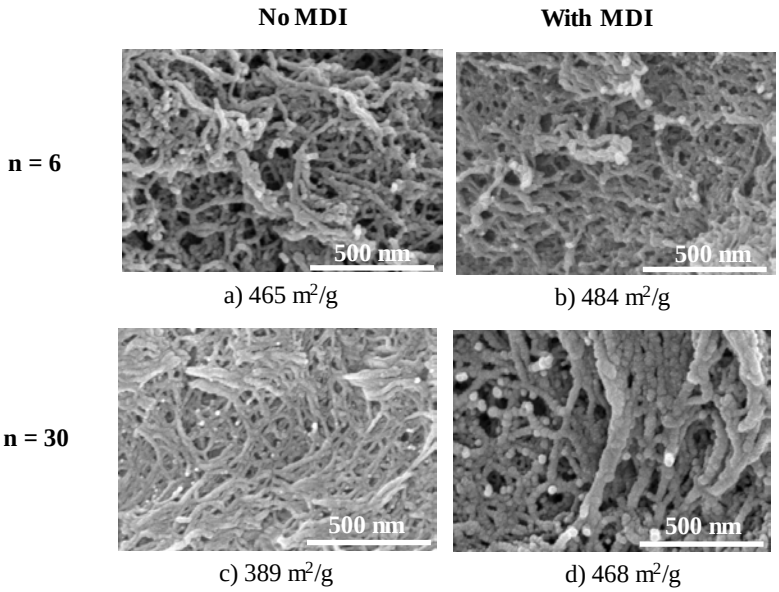

Figure 5. SEM of polyimide and poly(imide-urea) aerogels at a and b) n of 6, c and d) n of 30, respectively.

Listed in Tables 1 and 2 are mechanical properties including compressive, tensile moduli and specific moduli of the PI and PIU aerogels, measured on cylindrical monoliths and aerogel films, respectively. Shown in Figure 6a is the stress-strain curves of PI and PIU aerogel monoliths with n = 6 and n = 30. The compressive modulus, or Young's modulus, is obtained from the initial slope of the elastic linear region. Figure 6b is the plot of compressive modulus as a function of the chain length. In comparison to the PI aerogels, the PIU aerogels exhibit lower moduli due to lower densities. As found in other work previously reported,[28,47] moduli obtained for both PI and PIU aerogels are density dependent, and that higher modulus is obtained at higher n value, or its higher corresponding density. The plot of specific modulus, compressive modulus over bulk density, is presented in Fig. 6c, verifies the modulus-density relationship over the range of n values.

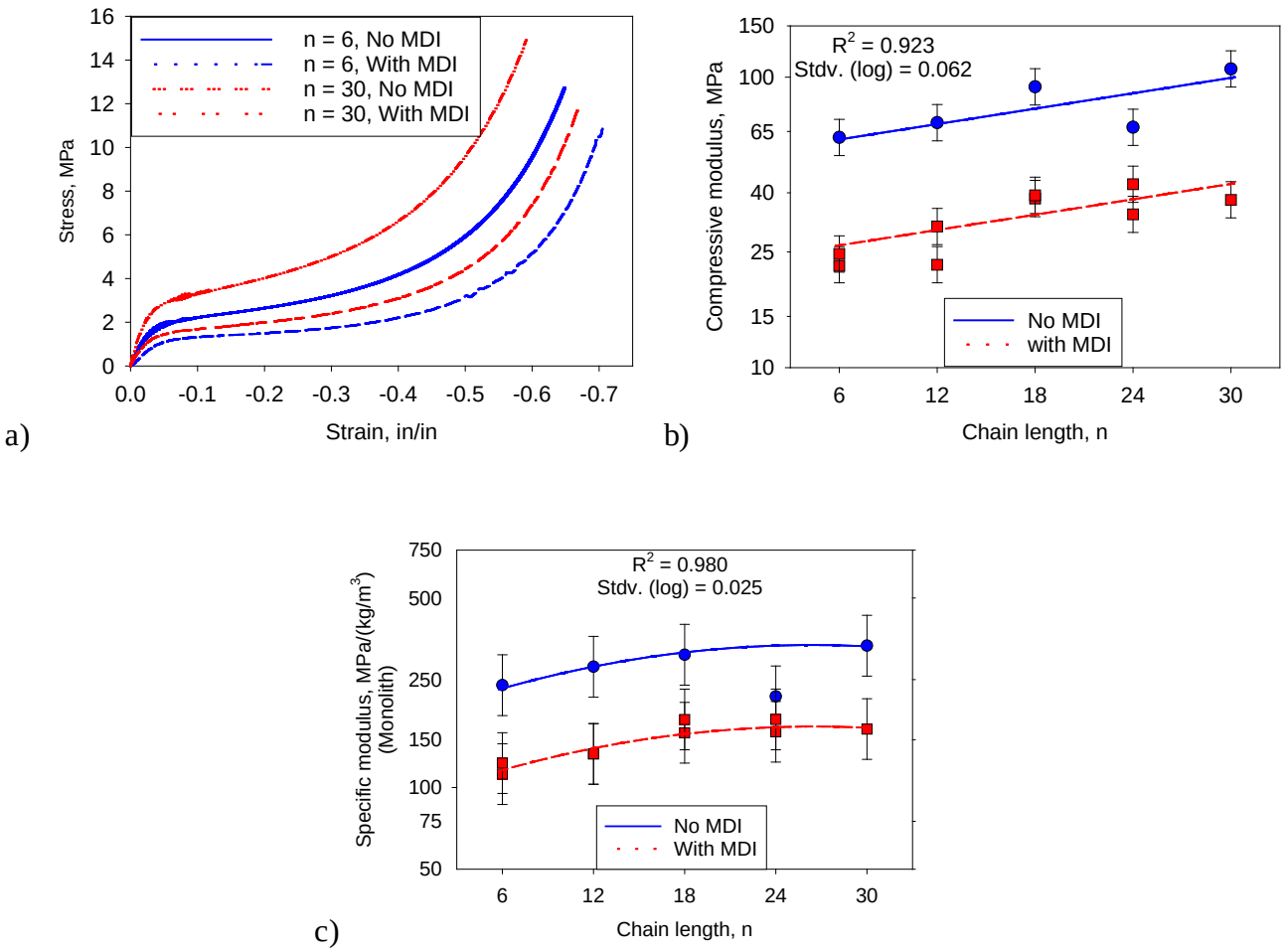

Figure 6. Graphs of a) stress-strain curve of n = 6 and n = 30, b) compressive modulus, and c) log-log plot of density *vs*. modulus of PI aerogels and PIU aerogels. The lines and error bars on the plots are derived from multiple linear regression analysis of the entire dataset.

The PI and PIU aerogels were also fabricated into thin films as described. Chuang *et. al.* [48] reported that the inherent viscosity of the BAPP-BTDA poly(amic acid) solution was initially high, but was remarkedly reduced upon the conversion to polyimide. The same phenomenon was observed in the fabrication of PI aerogels. A drastic decrease in viscosity occurred shortly after the addition of acetic anhydride and pyridine as the poly(amic acid) converted to polyimide. The viscosity of the polyimide solution remained low over the first 47-48 min., then thickened rapidly before gelation took place after about 50 minutes, allowing only a narrow minute of widow of film casting. Hence, only a 3″ x 6″ PI aerogel films were obtained. In contrast, the poly(amic acid)-urea solution was lower than the poly(amic acid) solution before being cross-linked with TAB, but steadily increased once

acetic anhydride and pyridine were added. Gelation occured after about 25 minutes but the viscosity was at a suitable level for film casting for approximately 10-15 minutes before the gelation point. As a result, large PIU aerogel films could be cast on pilot scale. Shown in Figure 7 is a picture of a 7″ x 12″ sheet, cut off from a roll 12″ x 5′ roll of PIU aerogel film. The difference in viscosity between PI and PIU solutions was due to the hydrogen bonds from urea links derived from reaction of MDI and BAPP, which further strengthened and preserved the pores within the network, even at a small MDI quantity. A similar trend in density is observed in both films and monoliths, and that higher n values result in higher density as well as PIU aerogel films exhibits lower density compared to their PI analogs. However, due to the greater surface area to thickness ratios when exposed to air which caused the pores to collapse, the films exhibited higher density compared to their monolith analogs, as illustrated in Figure S2. The inclusion of the MDI into the polyimide backbone led to better film forming during the casting process on pilot scale. Thus, the large, flexible PIU aerogel films would possibly be used to wrap around subjects of different shapes and sizes.

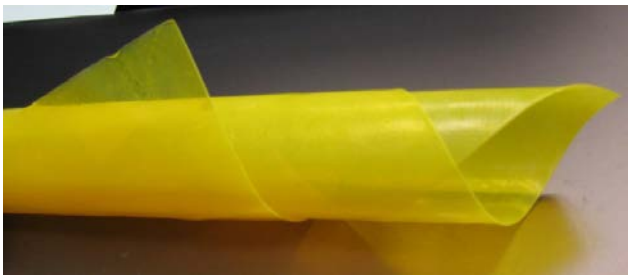

Figure 7: Poly(imide-urea) aerogel film.

Figure 8a shows graphs of the stress-strain curves of PI and PIU aerogel films with n = 6 and n = 30. As observed, the PIU aerogel films exhibited lower tensile stress as well as shorter elongation at break (% strain) than those of their corresponding PI aerogel films, an indication that the insertion of MDI on the polyimide chains led to a decrease in the flexibility due to the urea linkage, particularly at lower n due to higher MDI concentration. Illustrated in Figure 8b is the film tensile modulus which increases with increasing n, a trend directly correlated with their density (Fig. S2) and in agreement with the specific modulus as graphed in Figure 8c as well.

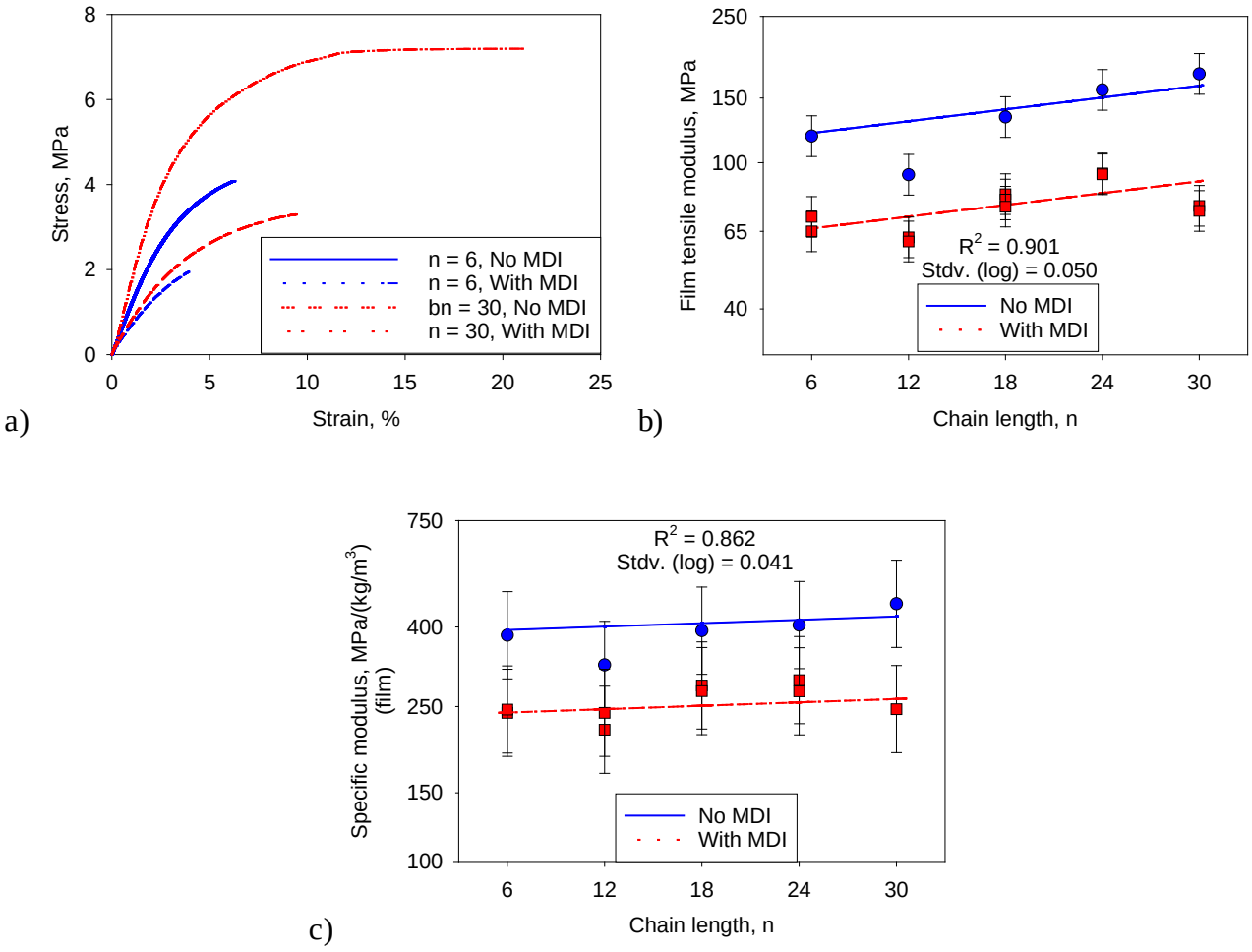

Figure 8. Graphs of a) stress-train curve of n = 6 and n = 30, b) film tensile modulus and c) tensile modulus *vs.* density of PI and PIU aerogel film. The lines and error bars on the plots are derived from multiple linear regression analysis of the entire dataset.

Figures 9 (a and b) shows thermal gravimetric analysis of PIs and PIUs with n values of 6, 18 and 30, respectively. The TGA curves shows a weight loss of 0.4 – 0.6 % at around 200 °C for all the aerogel specimens, likely due to some incomplete imidization. As shown in Figure 9a, the onsets of decomposition for PI aerogels made with different values of n are very similar, at about 520 °C, while in Figure 9b, the onsets of decomposition and degree of weight loss starting at 300 °C for PIU aerogels are quite different. The earlier onset is due to the

presence of urea in the backbone. As n increases, weight loss decreases due to the decreasing amount of urea in the overall backbone.

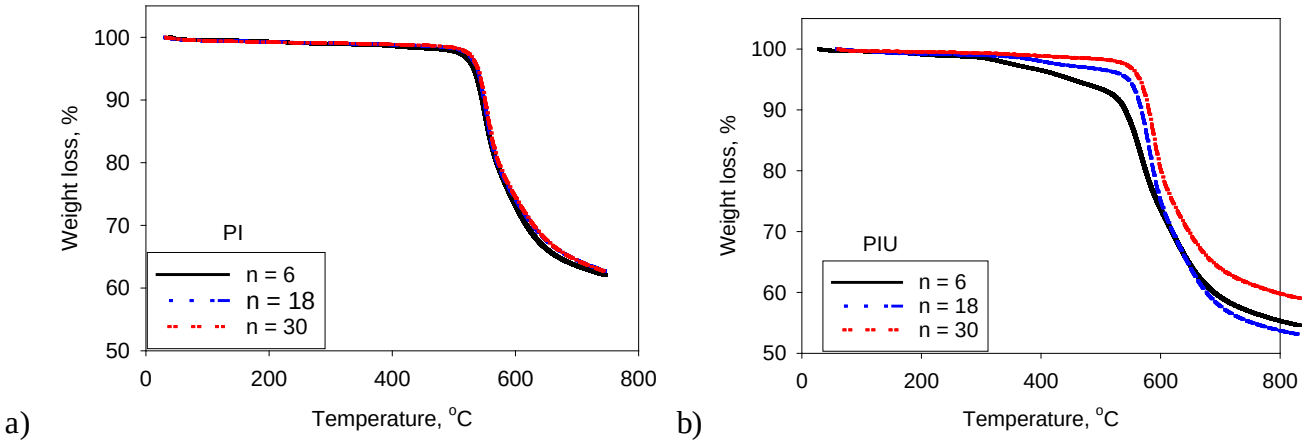

Figure 9. TGA curves of a) cross-linked polyimide and b) cross-linked poly(imide-urea) aerogels.

Dimensional stability of the PI and PIU aerogels was evaluated and compared by isothermally aging specimens for 500 hours at 150 °C and 200 °C in air. Areal shrinkage of the aerogel specimens was measured periodically during the aging. An insignificant amount of weight loss, <1 wt %, was detected during the aging as expected since these temperatures are below the onsets of decomposition as shown by TGA. The small weight loss may be due to loss of water due to some incomplete imidization, or loss of residual NMP. At elevated temperatures, the aerogels all shrank noticeably during the first 24 hours, then maintained the same dimensions for up to 500 hours. Graphed in Figure S3-a and Figure S3-b are plots of the areal shrinkage of the PI and PIU aerogels at 150 °C and 200 °C with n = 6 and n = 30. In general, the areal shrinkage is higher with higher n values, likely due to a decrease in crosslink density. It was found that PIU aerogels exhibited less shrinkage than their PI aerogels counterparts, perhaps due to the hydrogen bonding from urea as an additional secondary cross-linker. Thus, the lowest shrinkage is observed for PIU aerogels made using n = 6

Conclusions

Two sets of polyimide and poly(imide-urea) aerogels with polyimide backbones based on BTDA and BAPP and cross-linked with TAB were fabricated and characterized. Both PI and PIU aerogels were prepared at 10 wt%

in solution and with repeat units, n, ranging from 6 to 30. The PIU aerogels were formulated from an analogous PI aerogel backbone with 4,4'-methylene diphenyl di-isocyanate (MDI) added. The inclusion of urea derived from MDI in the polyimide backbone also results in an aerogel skeleton more resistant to shrinkage most likely due to virtual crosslinking from hydrogen bonding, leading to lower shrinkages, lower densities, higher % porosities and higher BET surface areas compared to their polyimide aerogel counterparts. As a result, PIU exhibited lower compressive and tensile moduli. For films casting, the PI solutions remained at constantly low viscosity upon the conversion of amic acid to imide before the gelation point, thus offering a narrow window of processing. The addition of the urea link in the polyimide backbone contributed to a faster built up in viscosity of the PIU solution, and larger window to cast film, thus, enabling fabrication of larger films and film forming. The capability to process flexible PIU film casting on pilot scale offers a potential market at an affordable cost for aerospace applications such as inflatable decelerators and extra-vehicular activity (EVA) space suits, as well as terrestrial goods including clothing, pipe wrapping, and other items of different shapes and sizes Both the PI and PIU aerogels were thermally stable at 150 °C and 200 °C for 500 hours, showing negligible (<1%) weight loss, but significant dimensional shrinkage was observed in the first 24 hours of aging.

Acknowledgement. Financial support from NASA's Fundamental Aeronautics Program is gratefully acknowledged. The authors also thank Ms. Anna Palczer and Dr. Haiquan Guo for the BET surface area data.

References

[1] Kistler, S. S.; Caldwell, A. G. Thermal Conductivity of Silica Aerogel. *Ind. Eng. Chem.* **1934**, *26 (6)*, 658-662.

[2] Hüsing, N.; Schuber, U. Aerogels – Airy Materials: Chemistry, Structure, and Properties. *Angew. Chem. Int. Ed.* **1998**, *37*, 22-45.

[3] Pajonk, G. M. Aerogel Catalysts. *Appl. Catalysis*, **1991**, *72*, 217-266.

[4] Pekala, R. W.; Schaefer, D. W. Structure of Organic Aerogels. 1. Morphology and Scaling. *Macromolecules*, **1993**, *26*, 5487-5493.

[5] Jo, M-H.; Hong, J-K.; Park, H-H.; Kim, J-J.; Hyun, S-H.; Choi, S-Y. Application of SiO2 Aerogel Film with Low Dielectric Constant to Intermetal Dielectrics. *Thin Solid Films*, **1997**, *308-309*, 490-494.

[6] Meador, M. A. B.; McMillon, E.; Sandberg, A.; Barrios, E.; Wilmoth, N. G.; Mueller, C. H.; Miranda, F. A. Dielectric and Other Properties of Polyimide Aerogels Containing Fluorinated Blocks. *ACS Appl. Mater. Interfaces*, **2014**, *6*, 6062-6068.

[7] Cuce, E.; Cuce, P. M.; Wood, C. J.; Rffat, S. B. Toward Aerogel Based Thermal Superinsulation in Buildings: A Comprehensive Review. *Renew. Sust. Energy Rev.*, **2014**, *34*, 273-299.

[8] Xu, X.; Zhang, Q.; Hao, M.; Hu, Y.; Lin, Z.; Peng, L.; Wang, T.; Ren, X.; Wang, C.; Zhao, Z.; Wan, C.; Fei, H.; Wang, L.; Zhu, J.; Sun, H.; Chen, W.; Du, T.; Deng, B.; Cheng, G. J.; Shakir, I.; Dames, C.; Fisher, T. S.; Zhang, Xl; Li, H.; Huang, Y.; Duan, X. Double-Negative-Index Ceramic Aerogels for Thermal Superinsulation. *Science*, **2019**, *363*, 723-727.

[9] Randall, J. P.; Meador, M. A. B.; Jana, S. C. Tailoring Properties of Aerogels for Aerospace Applications. *ACS Appl. Mater. Interfaces.* **2011**, *3 (3)*, 613-626.

[10] Meador, M. A. B.; Miranda, F. A. Glenn Research Center, Cleveland, Ohio. Design and Development of Aerogel-Based Antennas for Aerospace Application: A Final Report to the NARI Seedling, 2014, NASA/TM-2014-218346.

[11] Dorcheh, A. S.; Abbasi, M. H. Silica Aerogel; Synthesis, Properties and Characterization. *J. Mater. Process. Tech.*, **2008**, *199 (1-3)*, 10-26.

[12] Lei, W.; Mochalin, V.; Liu, D.; Qin, S.; Gogotsi, Y.; Chen, Y. Boron Nitride Colloidal Solutions, Ultralight Aerogels and Freestanding Membranes Through One-Step Exfoliation and Functionalization. *Nat. Commun.*, **2015**, *6*, 8849-8856.

[13] Hayase, G. Nonomura, K.; Hasegawa, G.; Kanamori, K. Nakanishi, K. Ultralow-Density, Transparent, Superamphiphobic Boehmite Nanofiber Aerogels and Their Alumina Derivatives. *Chem. Mater.*, **2015**, *27 (1)*, 3-5.

[14] Wang. X.; Jana, S. C. Synergistic Hybrid Organic-Inorganic Aerogels. *ACS Appl. Mater. Interfaces*, **2013**, *5 (13)*, 6423-6429.

[15] Nguyen, B. N.; Meador, M. A. B.; Medoro, A.; Arendt, V.; Randall, J.; McCorkle, L. Shonkwiler, B. Elastic Behavior of Methyltrimethoxysilane Based Aerogels Reinforced with Tri-Isocyanate. *ACS Appl. Mater. Interfaces*, **2010**, *2 (5)*, 1430-1443.

[16] Guo, J.; Nguyen, B. N.; Li, L.; Meador, M. A. B.; Scheiman, D. A.; Cakmak, M. Clay Reinforced Polyimide/Silica Hybrid Aerogel. *J. Mater. Chem. A.*, **2013**, *1*, 7211-7221.

[17] Jirglová, H.; Pérez-Cadenas, A. F.; Maldonado-Hódar, F. J. Synthesis and Properties of Phloroglucinol-Phenol-Formaldehyde Carbon Aerogels and Xerogels. *Langmuir*, **2009**, *25*, 2461-2466.

[18] Pekala, R. W.; Farmer, J. C., Alviso, C. T.; Tran, T. D.; Mayer, S. T.; Miller, J. M.; Dunn, B. Carbon Aerogels for Electrochemical Applications, *J. of Non-Cryst. Solids* **1998**, *225*, 74-80.

[19] Morales-Torres, S.; Maldonado-Hódar, F. J.; Pérez-Cadenas, A. F.; Carrasco-Marín, F. Textural and Mechanical Characteristics of Carbon Aerogels Synthesized by Polymerization of Resorcinol and Formaldehyde Using Alkali Carbonates as Basification Agents. *Phys. Chem. Chem. Phys.*, **2010**, *12*, 10365-10372,

[20] Zhu, C.; Han, T. Y-J.; Duoss, E. B.; Gobobic, A. M.; Kuntz, J. D.; Spadaccini, C. M.; Worsley, M. A. Highly Compressible 3D Periodic Graphene Aerogel Microlattices. *Nature Commun.*, **2015**, 6, 6962-6969,

[21] Xiao, J.; Tan, Y.; Song, Y.; Zheng, Q. A Flyweight and Superelastic Graphene Aerogel as a High-Capacity Adsorbent and Highly Sensitive Pressure Sensor. *J. Mater. Chem. A.*, **2018**, *6*, 9074-9080.

[22] Cai, H.; Sharma, S.; Liu, W.; Mu. W.; Liu, W.; Zhang, X.; Deng, Y. Aerogel Microspheres from Natural Cellulose Nanofibrils and Their Application as Cell Culture Scaffold. *Biomacromolecules*, **2014**, *15*, 2540-2547,

[23] Zeng, Z.; Ma, X. Y. D.; Zhang, Y.; Wang, Z.; Ng, B. F.; Wan, M. P.; Lu, X. Robust Lignin-Based Aerogel Filters: High Efficientcy Capture of Ultrafine Airborn Particulates and the Mechanism. *ACS Sust. Chem. Eng*., **2019**, *7*, 6959-6968.

[24] Daniel, C.; Sannino, D.; Guerra, G. Syndiotactic Polystyrene Aerogels: Adsorption in Amorphous Pores and Absoption in Crystalline Nanocavities. *Chem. Mater*. **2008**, *20*, 577-582.

[25] Mohite, D. P.; Mahadik-Khanolkar, S. M.; Luo, H.; Lu, H.; Sotiriou-Leventis, C.; Leventis, N. Polydicyclopentadiene Aerogels Grafted with PMMA: I. Molecular and Interparticle Crosslinking. *Soft Matter*, **2013**, *9 (5)*, 1516-1530.

[26] Wang, X.; Jana, S. C. Syndiotactic Polystyrene Aerogels Containing Multi-Walled Carbon Nanotubes. *Polymer*, **2013**, *54*, 750-759,

[27] Arndt, E. M.; Gawryla, M. D.; Schiraldi, D. A.; Elastic, Low Density Epoxy/Clay Aerogel Composites. *J. Mater. Chem.*; **2007**, *17*, 3525-3529,

[28] Nguyen, B. N.; Meador, M. A. B.; Scheiman, D.; McCorkle, L. Polyimide Aerogels Using Triisocyanate as Cross-Linker. *ACS Appl. Mater. Interfaces*, **2017**, *9*, 27313-27321.

[29] Vivod, S. L.; Meador, M. A. B.; Pugh, C.; Wilkosz, M.; Calomino, K.; McCorkle, L. Toward Improved Optical Transparency of Polyimide Aerogels. *ACS Appl. Mater. Interfaces*, **2020**, *12 (7)*, 8622-8633.

[30] Lin, Y.; Chen, C.; Hu, S.; Zhang, D.; Wu, G. Facile Fabrication of Mechanically Strong and Thermal Resistant Polyimide Aerogels with an Excess of Cross-linker. *J. Mater. Res. Tech.*, **2020**, *9 (5)*, 10719-10731.

[31] Guo, H.; Meador, M. A. B.; McCorkle, L.; Quade, D. J.; Guo, J.; Hamilton, B.; Cakmak, M. Tailoring Properties of Cross-Linked Polyimide Aerogels for Better Moisture Resistance, Flexible and Strength. *ACS Appl. Mater. Interfaces*, **2012**, *4*, 5422-5429.

[32] Pantoja, M.; Boynton, N.; Cavicchi, K. A.; Dosa, B.; Cashman, J. L.; Meador, M. A. B. Increased Flexibility in Polyimide Aerogels using Aliphatic Spaces in the Polymer Backbone. *ACS Appl. Mater. Interfaces*, **2019**, *11*, 9425-9437.

[33] Guo, H.; Meador, M. A. B.; Cashman, J. L.; Tresp, D.; Dosa, B.; Scheiman, D. A.; McCorkle, L. S. Flexible Polyimide Aerogels with Dodecane Links in the Backbone Structure. *ACS Appl. Mater. Interfaces*, **2020**, *12 (29)*, 33288-33296.

[34] Cashman, J. L.; Nguyen, B. N.; Dosa, B.; Meador, M. A. B. Flexible Polyimide Aerogels Derived from the Use of a Neopentyl Spacer in the Backbone. *ACS Appl. Polym. Mater.*, **2020**, *2*, 2179-2189.

[35] Meador, M. A. B.; McMilon, E.; Sandberg, A.; Barrios, E.; Wilmoth, N. G.; Mueller, C. H.; Miranda, F. A. Dielectric and Other Properties of Polyimide Aerogels Containing Fluorinated Blocks. *ACS Appl. Mater. Interfaces*. **2014**, *6*, 6062-6068.

[36] Guo, H.; Meador, M. A. B.; McCorkle, L.; Quade, D. J.; Guo, J.; Hamilton, B.; Cakmak, M.; Sprowl, G. Polyimide Aerogels Cross-Linked through Amine Functionalized Polyoligomeric Silsequioxane. *ACS Appl. Mater. Interfaces*, **2011**, *3*, 546-552.

[37] Del Corso, J. A.; Cheatwood, F. M.; Bruce, W. E.; Hughes, S. J.; Calomino, A. M. Presented at the *21st AIAA Aerodynamic Decelerator Systems Technology Conference and Seminar*, Dublin, Ireland, May 23-26, 2011; AIAA: Reston, VA, 2011, Paper No. 2510.

[38] Kawagishi, K.; Saito, H.; Furukawa, H.; Horie, K. Superior Nanoporous Polyimides via Supercritical CO_2 Drying of Jungle-Gym-Type Polyimide Gels. *Macromol. Rapid Commun.*, **2007**, *28*, 96-100.

[39] Shen, D.; Liu, J.; Yang, H.; Yang, S. Highly Thermally Resistant and Flexible Polyimide Aerogels Containing Rigid-Rod Biphenyl, Benzimidazole, and Triphenylpyridie Moieties: Synthesis and Characterization. *Chem. Lett.*, **2013**, *42*, 1545-1547.

[40] Meador, M. A. B.; Alemán, C. R.; Hanson, D.; Ramirez, N.; Vivod, S. L.; Wilmoth, N.; McCorkle, L. Polyimide Aerogels with Amide Cross-links: A Low Cost Alternative for Mechanically Strong Polymer Aerogels. *ACS Appl. Mater. Interfaces.* **2015**, *7*, 1240-1249.

[41] Guo, H.; Meador, M. A. B.; McCorkle, L.; Scheiman, D. A.; McCrone, J. D. and Wilkewitz, B. Synthesis and Characterization of Poly(maleic anhydride) Cross-linked Polyimide aerogels. *RSC Adv.*, **2016,** *6*, 26055-26065

[42] Kawagishi, K.; Saito, H.; Furukawa, H.; Horie, K. Superior Nanoporous Polyimides via Supercritically CO2 Drying of Jungle-Gym-Type Polyimide Gels. *Macromol. Rapid Commun.*, **2007**, *28*, 96-100.

[43] Kim, J.; Kwon, J.; Kim, M.; Do, J.; Lee, D.; Han, H. Low-Dielectric-Constant Polyimide Aerogel Composite Films with Low Water Uptake. *Polym. J.*, **2016**, *48*, 829-834.

[44] Meador, M. A. B.; Malow, E. J.; Silva, R.; Wright, S.; Quade, D.; Vivod, S. L.; Guo, H.; Guo, J.; Cakmak, M. Mechanical Strong, Flexible Polyimide Aerogels Cross-Linked with Aromatic Triamine. *ACS Appl. Mater. Interfaces*, **2012**, *4*, 536-544.

[45] Wu, S.; Du, A.; Huang, S.; Sun, W.; Xiang, Y.; Zhou, B. Solution-Processable Polyimide Aerogels with High Hydrophobicity. *Mater. Lett.*, **2016**, *176*, 118-121.

[46] Feng, L,; Iroh, J. O. Novel Polyimid-*b*-Polyurea Supramacromolecule with Remarkable Thermomechanical and Dielectric Properties. *Euro. Poly. J.* **2013**, *49*, 1811-1822.

[47] Shinko, A.; Jana, S. C.; Meador, M. A. Crosslinked Polyurea Aerogels with Controlled Porosity. *RSC Adv.* **2015**, 5, 105329.

[48] Chuang, K. C.; Scheiman, D. A.; Fu, J.; Crawford, M. Synthesis and Characterization of Polyimides with Ether Linkages. *J. Poly. Sci. Part A: Poly. Chem.* **1999**, *37*, 2559-2569.

[49] Seshadri, K. S.; Antonoplos, P. A.; Heilman, W. J.; 13C-NMR Spectroscopy of Polyamic Acids and Polyimide. *J. Polym. Sci.: Polym. Chem. Ed.* **1980**, *18*, 2649-2662.

[50] Jin, X.; Guo, N.; You, Z.; Tan, Y. Design and Performance of Polyurethane Elastomers Composed with Different Soft Segments. *Materials* **2020**, *13*, 4991.

[51] Giroto, A. S.; Valle, S. F.; Ribeiro, T.; Ribeiro, C.; Mattoso, L. H. C.; Towards Urea and Glycerol Utilizaation as "Building Blocks" for Polyurethane Production: A detailed Study about Reactivity and Structure for Environmentally Friendly Polymer Synthesis. *React. Func. Polym.* **2020**, *153*, 104629.

[52] Wolinska-Grabczyk, A.; Schab-Balcerzak, E.; Grabiec, E.; Jankowski, A.; Matlengiewicz, M.; Szeluga, U.; Kubica, P. Structure and Properties of New Highly Soluble Aromatic Poly(etherimide)s Containing Isopropylidene Groups. *Polym. J.*, **2013**, *45*, 1202-1209.

[53] Chung, C-H.; Shih, W-C.; Chiu, W-M. Synthesis, Characterization of Properties of Biomass and Carbon Dioxide Derived Polyurethane Reactive Hot-Melt Adhesive. *e-Polymers* **2019**, *19*, 535-544.

[54] Duff, D. W.; Maciel, G. E. ^{13}C and ^{15}N CP/MAS NMR Characterization of MDI-Polyisocyanurate Resin System. *Macromolecules* **1990**, *23*, 3069-3079.

[55] Raghu, A. V.; Gadaginamath, G. S.; Mallikarjuna, N. N.; Aminabhavi, T. M.; Synthesis and Characterization of Novel Polyureas Based on Benzimidazoline-2-one and Benzimidazonline-2-thione Hard Segments. *J. Appl. Polym. Sci.* **2006**, *100*, 576-583.

[56] Chidambareswarapattar, C. Larimore, Z.; Sotiriou-Leventis, C.; Mang, J. T.; Leventis, N. One-Step Room Temperature Synthesis of Fibrous Polyimide Aerogels from Anhydrides and *Isocyanates* and Conversion to Isomorphic Carbons. *J. Mater. Chem.* **2010**, *20*, 9666-9678.

[57] Toiserkani, H. Organosoluble and Thermally Stable of Benzazole-Containing Poly(Imide-Urea)s: One-Pot Synthesis and Characterization. *Open J. Poly. Chem.* **2011**, *1*, 1-9.

[58] Li, X-l;; Chen, D-j. Sunthesis and Characterization of Aromatic/Aliphatic Co-polyureas. *J. Appl. Poly. Sci.* **2008**, *109*, 897-902.

Table of Content